

Paper:

3D Measurement Using a Fish-Eye Camera Based on EPI Analysis

Kenji Terabayashi*, Toru Morita**, Hiroya Okamoto***, and Kazunori Umeda***

*Department of Mechanical Engineering, Faculty of Engineering, Shizuoka University
3-5-1 Johoku, Hamamatsu, Shizuoka 432-8561, Japan
E-mail: tera@eng.shizuoka.ac.jp

**Sony Corporation
2-15-3 Konan, Minato-ku, Tokyo 108-6201, Japan
E-mail: Toru.Morita@jp.sony.com

***Department of Precision Mechanics, Faculty of Science and Engineering, Chuo University
1-13-27 Kasuga, Bunkyo-ku, Tokyo 112-8551, Japan
E-mail: umeda@mech.chuo-u.ac.jp

[Received October 14, 2011; accepted February 16, 2012]

In car driving support systems and mobile robots, it is important to understand three-dimensional environment widely at once. In this paper, we use a fish-eye camera as a sensor to measure three-dimensional (3D) environments. This camera can take a wide-range and distortional image and can be easily mounted on cars. We propose a method for reconstructing 3D environment using fish-eye images based on Epipolar-Plane Image (EPI) analysis. This method enables easy and stable matching of feature points. The effectiveness of the proposed method is verified by experiments.

Keywords: fish-eye lens camera, three-dimensional (3D) measurement, Epipolar-Plane Image (EPI)

1. Introduction

There has been a variety of researches in recent years into car driving support systems and robot autonomy. In these fields of research, it is important to acquire a variety of environmental information, amongst which 3D information is particularly useful. Various sensors are used to acquire information on the external environment, and these sensor systems are desired to be inexpensive and simple. One method to obtain wide-range 3D information at once is the 3D measuring method using omnidirectional image sequences [1–3]. As sensors to obtain omnidirectional images, combination of a camera and a convex mirror [1, 2], and Ladybug2 sensor with six adjacent cameras [3] are used. However, these are specialized sensors which have a problem that their positions to be installed in a robot or a car are restricted.

For that reason, this study focuses on fish-eye cameras. Fish-eye cameras have an ultra-wide viewing angle of 180° or more. They can capture images of a wide area at once, and because they are comparatively small they can be easily mounted on a car or robot. Therefore, they

are installed in a car to be used in systems to provide the drivers with a bird's eye view image looking down upon the car [4–6, a]. In addition, the 3D measuring method using multiple fish-eye cameras has been proposed [7–10]. Since fish-eye cameras take images of a wide area at once, images taken with fish-eye cameras (hereafter, fish-eye images) are greatly distorted at the periphery. Therefore, compared to images taken by regular pinhole cameras, it is more difficult to use them for measurements.

This paper proposes a method for taking 3D measurements using multiple fish-eye images acquired with one fish-eye camera, taking into account distortion in fish-eye images. Diverse 3D measurement methods using multiple fish-eye cameras [7–10] have been proposed, but when considering to install the camera in a robot or car, 3D measurement with only one fish-eye camera is desirable from the viewpoint of installation space and cost. As a method to reconstruct 3D environment using one fish-eye camera, it has been proposed to input two fish-eye images measured from two different positions [11]. In this method, corresponding points between two fish-eye images are obtained using SIFT features [12] etc., and based on the correlations the 3D information on the measured environment and the relative position and direction of the camera that took the two images are estimated. This method has the advantage that it can be also used when the camera's movement is unknown, but because of the difficulty in finding corresponding points in the peripheral part of the images where distortion is high or in the occluded parts, its application to multiple input images is difficult.

This paper therefore aims to realize 3D measurements based on Epipolar-Plane Image (EPI) analysis [13, 14] with multiple fish-eye image input. In EPI analysis, the camera's movement is restricted to make fixed epipolar constraints between images, which facilitate the search for corresponding points. EPI analysis for wide-angled view cameras has been applied in omnidirectional cameras [15, 16], but has not been applied in fish-eye cameras.

We will outline in Section 2 the fish-eye camera's pro-

jection model. In Section 3, we will explain constraints in movements of fish-eye cameras and EPI generation from the fish-eye image sequence. In Section 4, we will propose a 3D measurement method based on EPI analysis that takes into account distortions in fish-eye images. In Section 5, we will verify the effectiveness of our proposed method through an accuracy evaluation test and a measurement test of an indoor 3D environment.

2. Overview of a Fish-Eye Camera

General pinhole camera models can be expressed as

$$r = \delta \tan \theta \quad (1)$$

using the angle θ [rad] between the optical axis of lens and the projection line from the measuring point to the lens, and the image's height (distance from the optical axis to the projection point) r [pixel]. δ is expressed as

$$\delta = \frac{f}{w} \quad (2)$$

where f expresses the focal distance [mm], and w the pixel size [mm].

In contrast to the pinhole camera, fish-eye lenses have different projection models depending on the design. Representative models are equidistant projection, which is expressed as

$$r = \delta \theta \quad (3)$$

and orthographic projection expressed as

$$r = \delta \sin \theta. \quad (4)$$

Due to precision differences in the manufacturing process, fish-eye projection methods do not strictly conform to the ideal projection method. For that reason, the fish-eye camera model is commonly expressed as follows, using the odd degree approximation obtained by a Taylor expansion of the projection model.

$$r = k_1 \theta + k_2 \theta^3 + k_3 \theta^5 + \dots \quad (5)$$

Here k_1, k_2, k_3 are the camera's internal parameters. When considering the deviation of the optical axis (c_u, c_v), the internal parameter I is

$$I = [k_1 \ k_2 \ k_3 \ c_u \ c_v]^T. \quad (6)$$

The internal parameter I can be estimated by observing known shape patterns such as straight lines [5].

3. EPI Generation Using a Fish-Eye Camera

EPI is an image of the epipolar plane in 3D spatio-temporal data formed by sequentially stacked images. In this research we obtain 3D information through image analysis of the EPI. In this section we explain a method to generate EPI from a sequence of fish-eye images taken by a fish-eye camera.

Because fish-eye images are greatly distorted, common

EPI generation methods for cameras that produce only slightly distorted images are difficult to apply directly to fish-eye cameras. In common methods, the camera is moved in a direction perpendicular to the camera's optical axis, and a sequence of images taken at fixed intervals is input to generate EPI. Then, from the sequentially stacked 3D spatio-temporal data, an image is extracted as EPI on a plane parallel to the temporal axis and the direction of travel. In this case, it is easy to find corresponding points between the input images because the measuring points included in the EPI are restricted on the EPI plane regardless of time. However, when this EPI generation method is applied to fish-eye images, there is no planar constraint described above due to great distortion in the fish-eye images.

In this study, we consider EPI generation for a fish-eye camera traveling in the optical axis direction. This method can be applied to such a case as a fish-eye camera fixed at the front of a car obtains images while moving forward in a straight line. In our proposed method, we generate EPI in the following process: i) input a sequence of fish-eye images taken at fixed intervals by a fish-eye camera moving into the optical axis direction, ii) create sequentially stacked 3D spatio-temporal data, and iii) extract an image on the plane containing the optical axis.

With cameras with little distortion, almost all EPIs are generated through the camera's movement in a direction perpendicular to the optical axis, and there is almost no EPI generated through the movement in the optical axis direction. In addition, we have not found any EPI generation method using fish-eye images.

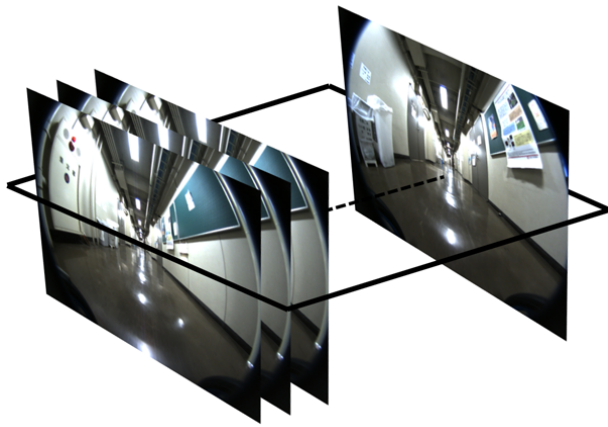
Figure 1 shows an example of EPI generation from a fish-eye image sequence. **Fig. 1(a)** shows an example of a fish-eye image sequence input for EPI generation and the plane including the optical axis. **Fig. 1(b)** shows the EPI corresponding to the plane.

A fish-eye camera can take a image of a wide area at once, and this means at the same time that a moving camera can capture the same measuring point in a wide area over a long time. This is an advantage of EPI analysis using a fish-eye camera. In the EPI shown in **Fig. 1(b)**, we can see curved lines which appeared because the fish-eye camera captured the same measuring point throughout an ultra-wide angled area. For this reason, we can expect to realize, through EPI analysis using a fish-eye camera, wide-area 3D measurements that are difficult to take with regular cameras.

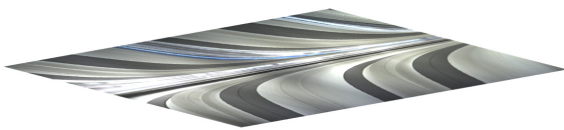
4. 3D Measurements Based on EPI Analysis of Fish-Eye Images

We propose a method for 3D measurements through image analysis of EPI generated from a fish-eye image sequence. Since EPI contains spatio-temporal information of the same measuring points in the fish-eye image sequence, 3D information is obtained from the trajectory of measuring points on the EPI.

With our proposed method, EPI is generated on the



(a) Fish-eye image sequence with epipolar plane



(b) Generated EPI

Fig. 1. Generation of Epipolar-Plane Image (EPI) from fish-eye images.

plane that includes the fish-eye camera’s optical axis. Each EPI obtained with the optical axis as the rotation axis is processed as follows. First, edge detection is carried out to track the trajectories of the measuring points included in the EPI. Then, the trajectory’s spatio-temporal gradient is calculated. Lastly, depth is calculated from this gradient information to obtain the 3D information.

In Section 4.1, we describe the image processing for edge detection and measuring point tracking in EPI. In Section 4.2, we explain how to calculate the spatio-temporal gradient with sub-pixel accuracy. In Section 4.3, we develop an equation for 3D measurement calculation that takes into account distortion in fish-eye images.

4.1. Tracking Measuring Points

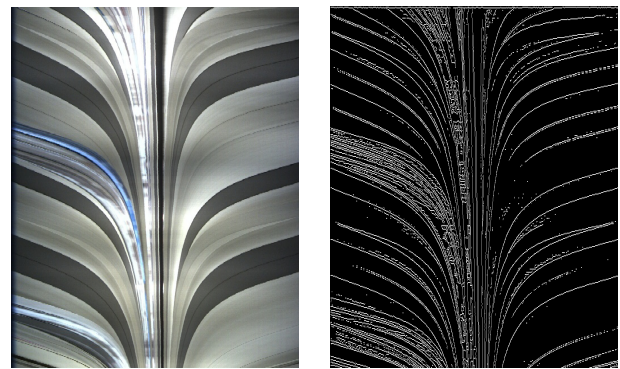
After detecting the edges in EPI, we use the connecting information to track the spatio-temporal trajectory of measuring points generated by the camera’s movement.

For edge detection in EPI, we use Canny’s edge detection algorithm [17]. **Fig. 2** shows an example of edge detection, with **Fig. 2(a)** showing the input EPI and **Fig. 2(b)** showing the output binary image of the detected edges.

The edges are detected per pixel. By identifying the connectivity of the detected pixels, we track the measuring points appearing as trajectories on the EPI.

4.2. Calculating the Spatio-Temporal Gradient

The spatio-temporal gradients are calculated for the trajectory of measuring points in the EPI obtained by edge



(a) Input EPI (b) Detected edges

Fig. 2. Edge detection on EPI using Canny operator.

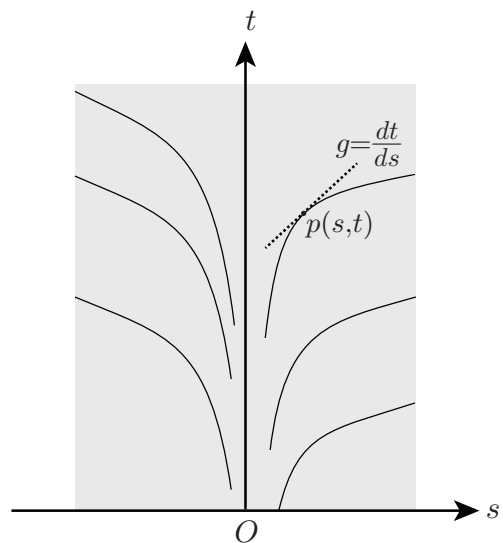


Fig. 3. EPI coordinate system and spatio-temporal gradient of a measuring point.

detection. For clarification, we define the EPI coordinate system as shown in **Fig. 3**. The abscissa s stands for the spatial direction and expresses the pixel position in the EPI’s cross-sectional direction. The ordinate t stands for the temporal direction and expresses the temporal sequence number of the fish-eye images.

We consider to make the gradient g for point $p(s,t)$ on the trajectory of the measuring point

$$g = \frac{dt}{ds} \dots \dots \dots (7)$$

to be linear approximation using the edge detection points neighboring $p(s,t)$. Concretely, the gradient g is approximated by the direction of the principal axis of the adjoining edge-detection points in the $t \pm \Delta t$ range.

Because the positions of the edge points detected using the Canny’s operator are of pixel accuracy, we improve the approximation accuracy of the spatio-temporal gradient g by estimating the edge positions in the s -axis direction with sub-pixel accuracy. Edge positions of sub-pixel accuracy are estimated as the zero crossing positions of the second derivatives of the intensity value of the EPI in s -direction.

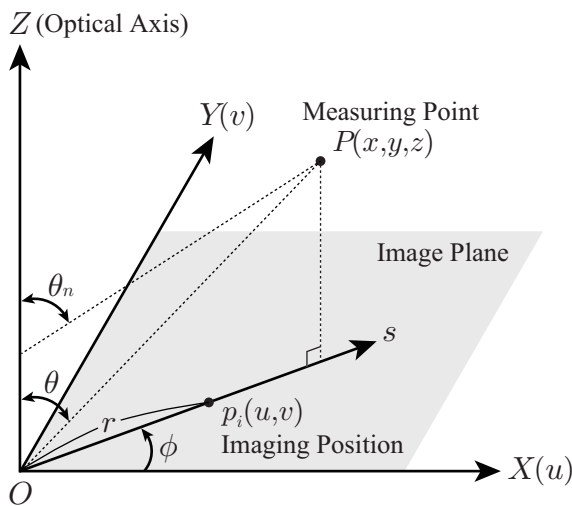


Fig. 4. 3D coordinate system.

Spatio-temporal gradient g includes the depth information. This can be understood in a qualitative manner as follows. The measuring point existing in a certain pixel position s travels on the EPI following the camera's movement. The displacement of the measuring point on the EPI depends on the distance between the camera and the measuring point; when the measuring point is far from the camera, the displacement is smaller compared to when the measuring point is close. Consequently, at the pixel position s where a certain distortion exist, the measuring point with high $|g|$ is far, and the measuring point with small $|g|$ is close.

4.3. 3D Measurements Tacking into Account Fish-Eye Image Distortion

We explain a 3D measuring method that takes into account distortions in fish-eye images, based on spatio-temporal gradient information calculated from EPI.

Here we consider the equidistant projection expressed in Eq. (3) as a fish-eye camera model. Equidistant projection is a representative projection model for fish-eye lenses, and is positioned as an approximate model for other projection models. Furthermore, equidistant projection parameters can be easily set based on the designed values of the camera and lens.

The 3D spatial coordinate system is defined as shown in Fig. 4. We consider to measure 3D positions (x,y,z) of point P , when the fish-eye camera, whose initial position is origin O , travels in the direction of the Z -axis (optical axis). The measuring direction θ , which is the angle between the optical axis Z and OP is

$$\theta = \tan^{-1} \frac{\sqrt{x^2 + y^2}}{z} \dots \dots \dots (8)$$

Similarly, if the shooting intervals are d_z , measuring direction θ_n at the shooting position number n is

$$\theta_n = \tan^{-1} \frac{\sqrt{x^2 + y^2}}{z - d_z n} \dots \dots \dots (9)$$

When the measuring point P in the 3D space is captured by a fish-eye camera and forms an image at the imaging position p_i with image coordinates (u, v) , the shooting direction ϕ for the imaging position p_i is

$$\phi = \tan^{-1} \frac{v}{u} \dots \dots \dots (10)$$

Furthermore, the image height r at the imaging position p_i is

$$r = \sqrt{u^2 + v^2} = s \dots \dots \dots (11)$$

equal to the coordinate value s of the spatial axis in the EPI in direction ϕ .

The curves in the EPI formed by measuring points $P(x,y,z)$ are

$$n = \frac{z \tan \frac{s}{\delta} - \sqrt{x^2 + y^2}}{d_z \tan \frac{s}{\delta}} \dots \dots \dots (12)$$

based on the relation among the projection model expressed in Eq. (3), the measuring direction θ_n in Eq. (9), and the image height r in Eq. (11). The spatio-temporal gradient g in the EPI is

$$g = \frac{dn}{ds} = \frac{\sqrt{x^2 + y^2}}{d_z \delta \sin^2 \frac{s}{\delta}} \dots \dots \dots (13)$$

In conclusion, the 3D positions (x,y,z) of the measuring point P can be calculated through

$$x = d_z \delta g \sin^2 \frac{s}{\delta} \cos \phi \dots \dots \dots (14)$$

$$y = d_z \delta g \sin^2 \frac{s}{\delta} \sin \phi \dots \dots \dots (15)$$

$$z = d_z \left(\frac{\delta g}{2} \sin \frac{2s}{\delta} + n \right) \dots \dots \dots (16)$$

using the spatio-temporal gradient g .

5. 3D Measuring Experiment

In this section we will verify the effectiveness of the 3D measuring method through EPI analysis using a fish-eye camera with two experiments: (1) an experiment to verify measurement accuracy in an environment where the positions to be measured are known, and (2) an experiment to apply the method to measurements in a real environment.

The fish-eye lens we used for these experiments was the TV1634M from Space Inc., and the camera was the Dragonfly2 (1024 pixel \times 768 pixel) from Point Grey Research, Inc. We used the designed values as follows: focal length $f = 1.6$ mm; pixel size $w = 4.65 \mu\text{m}$. The internal parameters of the fish-eye camera was $\delta = 344$. The fish-eye camera was fixed on an XY -stage as shown in Fig. 5, and the 3D measurements were taken from a sequence of images which were shot per movement with shooting pitch d_z [mm].

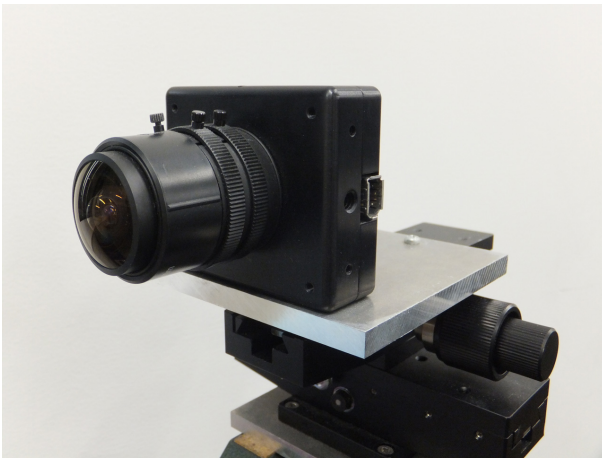


Fig. 5. Experiment system of a fish-eye camera on translation mechanics.

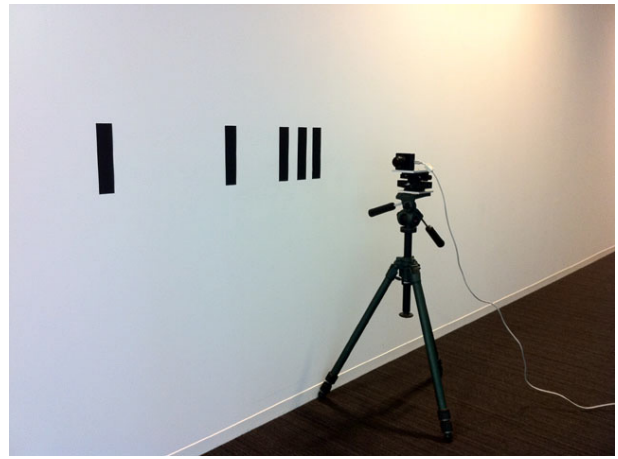


Fig. 7. Experimental scene for evaluation of measurement accuracy.

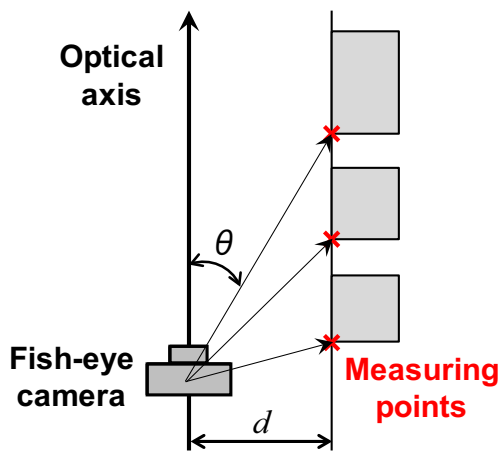


Fig. 6. Layout of a fish-eye camera and measuring points for evaluation of measurement accuracy.

5.1. Verification of Measurement Accuracy

In this section we verify the measurement accuracy using a known environment. For this verification, we simulated a situation where a car with an fish-eye camera moved in a straight line to measure a building facing the road. As illustrated in **Fig. 6**, we took the measurements while changing measuring direction θ and the scale d in the measurement environment.

Concretely, as shown in **Fig. 7**, the fish-eye camera's optical axis was arranged to be parallel with the wall, and a striped pattern on the wall was measured. There were five measuring directions θ of 15° , 30° , 45° , 60° and 75° , and seven measurement environment scale d of 200, 250, 300, 350, 400, 450 and 500 mm. We set the shooting pitch d_z [mm] at 10 mm for $d = 500$, and other scales d were set at the same ratio to be $d_z = d/50$.

Figure 8 shows the measurement results converted to the scale $d = 1000$ mm in an overhead view. For these measurements we used seven images to calculate the spatio-temporal gradients g in EPI. According to **Fig. 8**,

we can confirm that measuring points were obtained in a wide-angled area with $\theta = 60^\circ$ and 75° . This is an advantage of using a fish-eye lens, as it is difficult to take measurements in a wide area with a general camera represented by the pinhole camera model. It is also clear that when θ was 45° or 60° , measuring points close to the true value were obtained. On the other hand, errors increased when θ was 15° , 30° or 75° , and there was high variability in measuring points when θ was 15° .

Figure 9 shows the measuring errors for the measuring direction θ and the distance r_θ in the measuring direction. The abscissa is measuring direction θ [deg], the ordinate in **Fig. 9(a)** is the error of the measuring direction θ [deg], and the ordinate in **Fig. 9(b)** is the error ratio [%] of the distance r_θ in the measuring direction. It is clear from **Fig. 9(a)** that there was about -2° deviation in the measuring direction θ , and that as θ increased the variability increased. **Fig. 9(b)** shows that, as θ increased, the error ratio of the distance r_θ in the measuring direction increased but the variability decreased.

Based on the fact that the measuring direction θ greatly varied in ultra-wide angled areas, we can think that the principal cause of the variability in θ is the relative drop in resolution in the peripheral part of the fish-eye images. The cause for the deviation in θ and r_θ can be the simplification of the fish-eye camera model and the difference in direction between the camera's optical axis and the wall. The cause for the variability in r_θ can be the distance from the fish-eye camera.

5.2. Application to Real Environment Measurements

In this section we apply the 3D measurement method through EPI analysis using a fish-eye camera to real environment measurements. We used a flight of stairs shown in **Fig. 10** as the measurement environment, with the fish-eye camera shooting at a pitch of $d_z = 8$ mm while traveling towards the stairs.

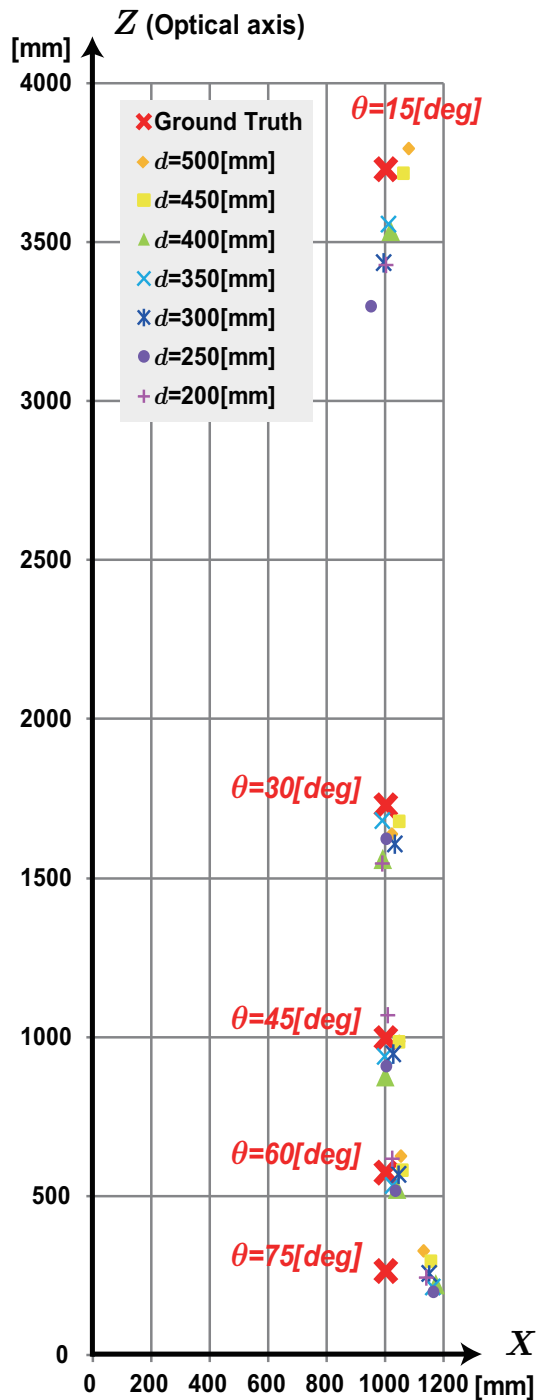
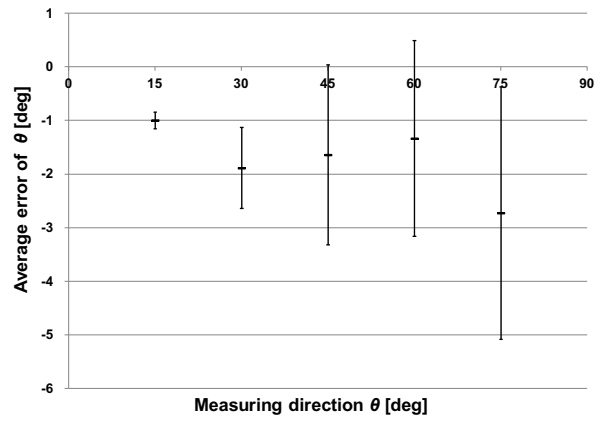
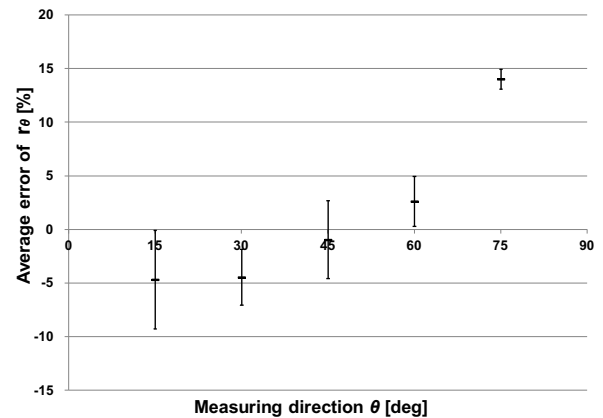


Fig. 8. Measured points and ground truth in overhead view.

Figure 11 shows the 3D measuring points in the stairs environment plotted on graphs. For these measurements we used five images to calculate the spatio-temporal gradient g on the EPI, and because the center of the fish-eye image was to be the camera's direction of travel, we eliminated points in measuring direction $\theta < 15^\circ$ as low-accuracy measuring points. Figs. 11(a)–(d) show the measuring points seen from an angle, on an XY-plane, an XZ-plane and a YZ-plane, respectively. The colors of the



(a) Measurement accuracy of θ



(b) Measurement accuracy of r_θ

Fig. 9. Measurement accuracy of average error with standard deviation.

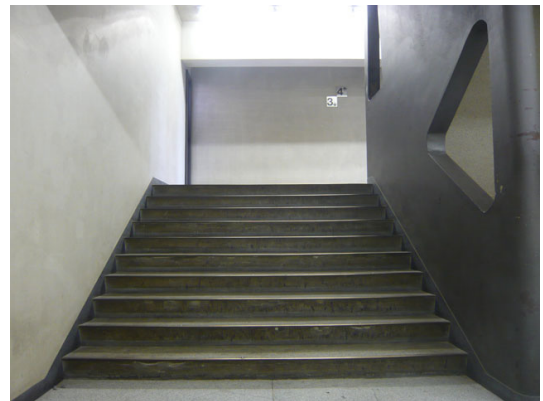


Fig. 10. Experimental scene of a stairs environment.

measuring points correspond to the distance to the optical axis direction.

By comparing Figs. 11(b) and 10, it is clear that environmental structures of edge parts were measured in such areas as the stairs (blue to light blue), the ceiling at the back of the stairs (red), two pillars at the right hand side (orange and blue).

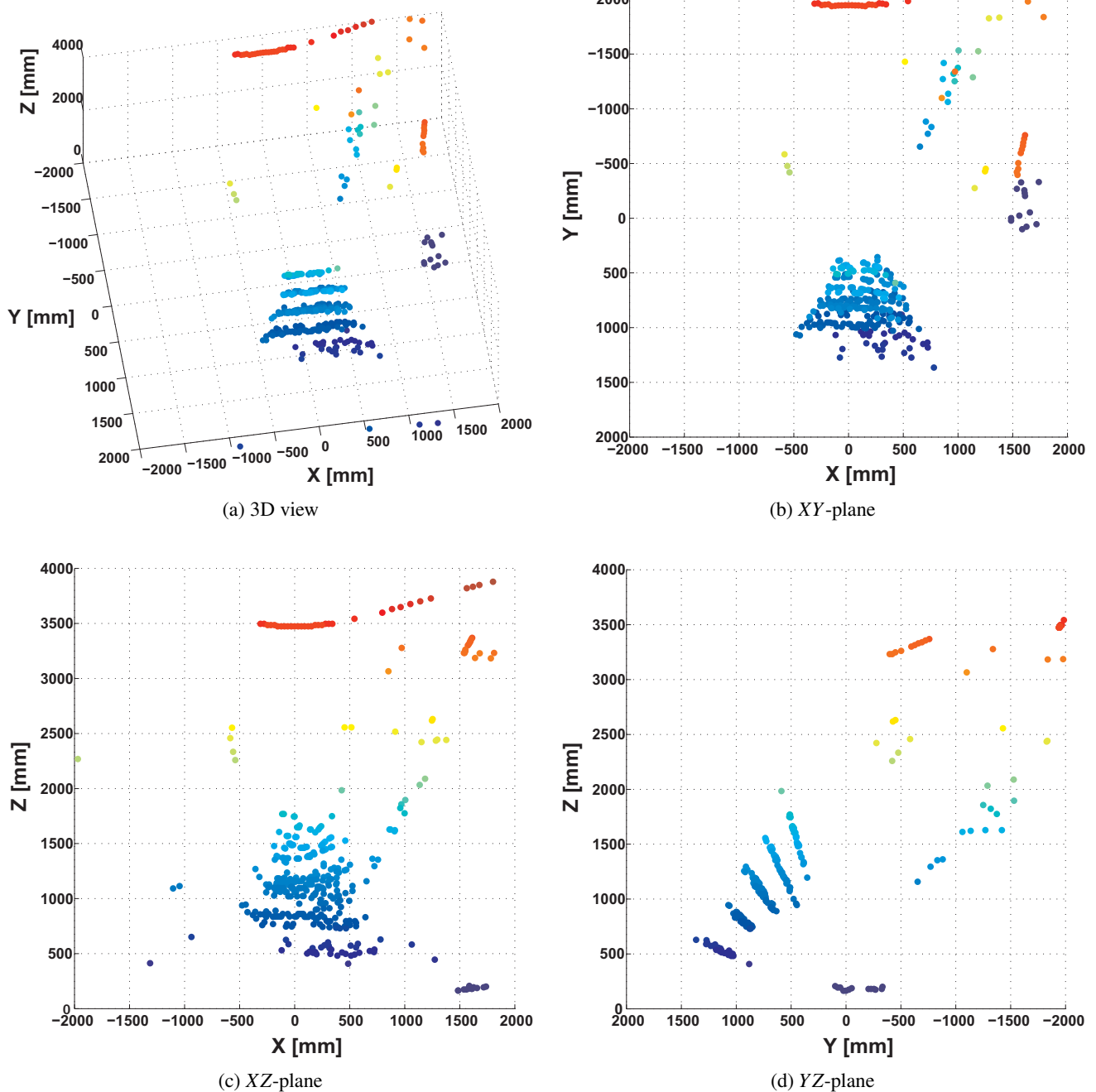


Fig. 11. Measurement result of a stairs environment.

6. Conclusion

This paper proposed a 3D measuring method through EPI analysis using a fish-eye camera. The distinctive feature of this method is the fact that EPI analysis is conducted using fish-eye images as they are, and thus image conversion using fish-eye parameters is not required. The accuracy verification and the application experiment in a real environment were carried out without camera parameter calibration. We only used the fish-eye camera and the camera's designed values to realize measurements in an ultra-wide angled area, and thus the effectiveness of the method was verified.

Future tasks include improvements in measurement accuracy using longer image sequences and easing of constraints on camera's movement.

References:

- [1] R. Bunschoten and B. Krose, "Robust scene reconstruction from an omnidirectional vision system," *IEEE Trans. on Robotics and Automation*, Vol.19, No.2, pp. 351-357, 2003.
- [2] R. Kawanishi, A. Yamashita, and T. Kaneko, "Three-Dimensional Environment Model Construction from an Omnidirectional Image Sequence," *J. of Robotics and Mechatronics*, Vol.21, No.5, pp. 574-582, 2009.
- [3] R. Matsuhisa, S. Ono, H. Kawasaki, A. Banno, and K. Ikeuchi, "Structure from Motion for omnidirectional images using efficient factorization method based on virtual camera rotation," *Proc. of Int.*

Workshop Computer Vision and Its Application to Image Media Processing, pp. 1-7, 2009.

- [4] L. Shigang, "Monitoring around a vehicle by a spherical image sensor," *IEEE Trans. on Intelligent Transportation Systems*, Vol.7, No.4, pp. 541-550, 2006.
- [5] R. Okutsu, K. Terabayashi, Y. Aragaki, N. Shimomura, and K. Umeda, "Generation of Overhead View Images by Estimating Intrinsic and Extrinsic Camera Parameters of Multiple Fish-Eye Cameras," *Proc. of IAPR Conf. on Machine Vision Applications (MVA)*, pp. 447-450, 2009.
- [6] Y. Chen, Y. Tu, C. Chiu, and Y. Chen, "An Embedded System for Vehicle Surrounding Monitoring," *Proc. of 2nd Int. Conf. on Power Electronics and Intelligent Transportation System (PEITS)*, Vol.2, pp. 92-95, 2009.
- [7] S. Abraham and W. Forstner, "Fish-eye-stereo calibration and epipolar rectification," *ISPRS J. of Photogrammetry and Remote Sensing*, Vol.59, pp. 278-288, 2005.
- [8] T. Nishimoto and J. Yamaguchi, "Three dimensional measurement using fisheye stereo vision," *Proc. of SICE Annual Conf. 2007*, pp. 2008-2012, 2007.
- [9] L. Shigang, "Binocular Spherical Stereo," *IEEE Trans. on Intelligent Transportation Systems*, Vol.9, pp. 589-600, 2008.
- [10] P. J. Herrera, G. Pajares, M. Guijarro, J. J. Ruz, and J. M. Cruz, "A Stereovision Matching Strategy for Images Captured with Fish-Eye Lenses in Forest Environments," *Sensors*, Vol.11, pp. 1756-1783, 2011.
- [11] K. Terabayashi, H. Mitsumoto, T. Morita, Y. Aragaki, N. Shimomura, and K. Umeda, "Measurement of Three Dimensional Environment with a Fish-eye Camera Based on Structure From Motion – Error Analysis," *J. of Robotics and Mechatronics*, Vol.21, No.6, pp. 680-688, 2009.
- [12] D. G. Lowe, "Object Recognition from Local Scale Invariant Features," *Proc. of IEEE Int. Conf. on Computer Vision (ICCV)*, pp. 1150-1157, 1999.
- [13] R. C. Bolles, H. H. Baker, and D. H. Marimont, "Epipolar-Plane Image Analysis: An Approach to Determining Structure from Motion," *Int. J. of Computer Vision*, Vol.1, pp. 7-55, 1987.
- [14] H. H. Baker and R. C. Bolles, "Generalizing epipolar-plane image analysis on the spatiotemporal surface," *Int. J. of Computer Vision*, Vol.3, No.1, pp. 33-49, 1989.
- [15] H. Kawasaki, K. Ikeuchi, and M. Sakauchi, "EPI analysis of omni-camera image," *Proc. of 15th IAPR Int. Conf. on Pattern Recognition (ICPR)*, Vol.1, pp. 379-383, 2000.
- [16] H. Kawasaki, K. Ikeuchi, and M. Sakauchi, "Spatio-Temporal Analysis of Omni Image," *Proc. of IEEE Computer Society Conf. on Computer Vision and Pattern Recognition (CVPR)*, Vol.2, pp. 577-584, 2000.
- [17] J. Canny, "A Computational Approach to Edge Detection," *IEEE Trans. on Pattern Analysis and Machine Intelligence*, Vol.8, No.6, pp. 679-698, 1986.

Supporting Online Materials:

- [a] Around view monitor. Nissan Motor [Online]. Available: <http://www.nissan-global.com/EN/TECHNOLOGY/OVERVIEW/avm.html>



Name:
Kenji Terabayashi

Affiliation:
Assistant Professor, Department of Mechanical Engineering, Faculty of Engineering, Shizuoka University

Address:
3-5-1 Johoku, Hamamatsu, Shizuoka 432-8561, Japan

Brief Biographical History:
2008 Received Ph.D. degree in Precision Engineering from The University of Tokyo
2008-2012 Assistant Professor, Chuo University
2012- Assistant Professor, Shizuoka University

Main Works:

- K. Terabayashi, H. Mitsumoto, T. Morita, Y. Aragaki, N. Shimomura, and K. Umeda, "Measurement of Three Dimensional Environment with a Fish-eye Camera Based on Structure From Motion – Error Analysis," *J. of Robotics and Mechatronics*, Vol.21, No.6, pp. 680-688, 2009.
- K. Terabayashi, Y. Hoshikawa, A. Moro, and K. Umeda, "Improvement of Human Tracking in Stereoscopic Environment Using Subtraction Stereo with Shadow Detection," *Int. J. of Automation Technology*, Vol.5, No.6, pp. 924-931, 2011.

Membership in Academic Societies:

- The Robotics Society of Japan (RSJ)
- The Japan Society for Precision Engineering (JSPE)
- The Japan Society of Mechanical Engineers (JSME)
- The Virtual Reality Society of Japan (VRSJ)
- The Institute of Electrical Engineers of Japan (IEEJ)
- The Institute of Image Electronics Engineers of Japan (IEEEJ)
- The Institute of Electrical and Electronics Engineers (IEEE)



Name:
Toru Morita

Affiliation:
Sony Corporation

Address:
2-15-3 Konan, Minato-ku, Tokyo 108-6201, Japan

Brief Biographical History:
2010 Received M.Eng. in Precision Engineering from Chuo University
2010- Joined Sony Corporation

Main Works:

- K. Terabayashi, H. Mitsumoto, T. Morita, Y. Aragaki, N. Shimomura, and K. Umeda, "Measurement of Three Dimensional Environment with a Fish-eye Camera Based on Structure From Motion – Error Analysis," *J. of Robotics and Mechatronics*, Vol.21, No.6, pp. 680-688, 2009.



Name:
Hiroya Okamoto

Affiliation:
Course of Precision Engineering, Graduate
School of Science and Engineering, Chuo Uni-
versity

Address:
1-13-27 Kasuga, Bunkyo-ku, Tokyo 112-8551, Japan

Brief Biographical History:
2012 Received B.Eng. in Precision Mechanics from Chuo University



Name:
Kazunori Umeda

Affiliation:
Professor, Department of Precision Mechanics,
Chuo University

Address:
1-13-27 Kasuga, Bunkyo-ku, Tokyo 112-8551, Japan

Brief Biographical History:
1994 Received Ph.D. degree in Precision Machinery Engineering from
The University of Tokyo
1994- Lecturer, Chuo University
2003-2004 Visiting Worker, National Research Council of Canada
2006- Professor, Chuo University

Main Works:

- N. Hikosaka, K. Watanabe, and K. Umeda, "Development of Obstacle Recognition System of Humanoids Using Relative Disparity Maps from Small Range Image Sensors," J. of Robotics and Mechatronics, Vol.19, No.3, pp. 290-297, 2007.
- M. Tateishi, H. Ishiyama, and K. Umeda, "A 200Hz Small Range Image Sensor Using a Multi-Spot Laser Projector," Proc. of IEEE Int. Conf. on Robotics and Automation, pp. 3022-3027, 2008.

Membership in Academic Societies:

- The Robotics Society of Japan (RSJ)
- The Japan Society for Precision Engineering (JSPE)
- The Japan Society of Mechanical Engineers (JSME)
- The Horological Institute of Japan (HIJ)
- The Institute of Electronics, Information and Communication Engineers (IEICE)
- Information Processing Society of Japan (IPSJ)
- The Institute of Electrical and Electronics Engineers (IEEE)